Supplement of Atmos. Chem. Phys., 19, 7129–7150, 2019
https://doi.org/10.5194/acp-19-7129-2019-supplement

Atmospheric Chemistry and Physics
Open Access

Supplement of

Experimental budgets of OH, HO_2, and RO_2 radicals and implications for ozone formation in the Pearl River Delta in China 2014

Zhaofeng Tan et al.

Correspondence to: Andreas Hofzumahaus (a.hofzumahaus@fz-juelich.de) and Yuanhang Zhang (yhzhang@pku.edu.cn)

Supplementary Text

Additional uncertainties in the budget analyses

Radical initiation by unmeasured VOCs

As pointed out in Section 4.1, unmeasured VOCs were most likely responsible for the observed missing OH reactivity. This not only considerably influences the radical chain propagation from OH to RO_2 (Fig. 3e, g), but can also affect the primary production of OH, HO_2, and RO_2 radicals. Unmeasured alkenes could form additional radicals through ozonolysis. Information about the abundance of alkenes in this campaign can be obtained from the $RO_2^{\#}$ budget analysis. $RO_2^{\#}$ is produced by OH reaction with alkenes, aromatics and large alkanes. The budget analysis (Fig. 3g, h) shows that the calculated production rate $P^{(1)}_{RO2\#}$ for $RO_2^{\#}$ from these compounds is balanced by the calculated $RO_2^{\#}$ loss rate. If an essential fraction of the unmeasured VOCs would consist of alkenes, it would increase the $RO_2^{\#}$ production rate correspondingly. Within experimental uncertainty, a doubling of the alkene contribution in the $RO_2^{\#}$ production would be acceptable without disturbing the balance in the $RO_2^{\#}$ budget. Doubling of the alkenes would explain 15% of the missing OH reactivity. In this case, the radical production from ozonolysis, which is less than 0.1 ppbv/h for OH and 0.05 ppbv/h for HO_2 at daytime, would increase by about a factor of 2. This increase would have a negligible impact on the radical budgets of OH and HO_2. Unmeasured OVOCs could form additional radicals (HO_2, RO_2) through photolysis. Such reactions would further increase the gap between the production and destruction rate for RO_2 and disturb the closed RO_x and HO_2 budgets.

Radical initiation by Cl atoms

Gaseous nitryl chloride ($ClNO_2$) can be formed at night by heterogeneous reaction of N_2O_5 with chloride in moist particles (e.g., Osthoff et al., 2008). In the morning, $ClNO_2$ photolyzes and forms Cl atoms which react very fast with VOCs and produce additional RO_2. This mechanism can play a role for 2 - 3 hours after sunrise until the $ClNO_2$ reservoir is depleted. $ClNO_2$ was not measured in Heshan, but was reported for other places in China. Measured concentrations shortly before sunrise are typically below 1 ppbv (e.g., Tham et al., 2016; Wang et al., 2018), but can occasionally reach a few ppb, e.g., 2.1 ppbv in Wangdu (Tham et al., 2016) and 4.7 ppbv in Hong Kong (Wang et al., 2016). With photolytical lifetimes of 2 - 3 hours, Cl production rates rarely exceed 0.5 ppbv/h. RO_2 production with a similar rate will make only a minor contribution to the RO_2 budget (Fig. 3e), and make the balance in the ROx budget slightly worse (Fig. 2g).

Uncertainties related to the measurement and chemistry of RO_2

Uncertainties in the radical budgets may be caused by the measurement and incomplete representation of the RO_2 chemistry. Due to the measurement principle of the applied ROxLIF technique, only those RO_2 species can be measured which are converted to HO_2 by reaction with NO. This measurement is exactly what is needed to quantify the HO_2 production rate (equation E5) in the atmospheric HO_2 budget. However, using the measured RO_2 data for the calculation of the RO_2 loss rate (equation E9) may cause a systematic bias. There exist RO_2 radical species which react with NO and produce a new RO_2 radical rather than HO_2. An example is the reaction $(CH_3)_3C(O_2)$+NO leading to CH_3O_2+acetone+NO_2 as products. The result is a low-biased measurement of atmospheric RO_2 radicals. Its use in equation E9 leads to an underestimation of D_{RO2} since the RO_2 loss leading to new RO_2 species is not included due to the measurement bias. On the other side, the production P_{RO2} in equation E8 is also underestimated by the same amount, because the production term for RO_2 species which are

produced by RO_2+NO is missing. As a result, the balance term D_{RO2}-P_{RO2} remains correct as the production and destruction terms are smaller by the same unknown amount. Another group of RO_2 radicals which are not well captured by ROxLIF are nitrate peroxy radicals which are formed by the reaction of NO_3 radicals with alkenes. Some nitrate peroxy radical species (e.g., from propene and butenes) react with NO and produce besides HO_2 in a parallel reaction carbonyl compounds and NO_2 as products. The latter reaction constitutes a ROx sink. In the present work, NO_3 reactions with VOCs play a minor role (Section 4.2.3).

Other uncertainties in the RO_2 budget are caused by the rate constants that are given in Table 1 as effective values for the lumped RO_2 radicals. It is well known that the rate coefficients for the reactions of RO_2 with NO, HO_2, and RO_2 depend on the chemical structure of the RO_2 species. According to Jenkin et al. (2019), experimentally known rate constants for RO_2+NO can be broadly categorized into three classes: [1] CH_3O_2 (C1), [2] other hydrocarbon (≥ C2) and oxygenated peroxy radicals, and [3] acyl peroxy radicals. At room temperature, recommended rate constants for these categories are 7.7×10^{-12} cm^3 s^{-1}, 9.0×10^{-12} cm^3 s^{-1}, and 2.0×10^{-11} cm^3 s^{-1}, respectively (Jenkin et al., 2019). The MCM value used in Table 1 for R8 + R14 (9.0×10^{-12} cm^3 s^{-1}) fits to the second class. The high rate constants for acyl peroxy radicals have no relevance for the budget analysis, because their reaction with NO produces another RO_2 radical. Thus, their reaction does not contribute to the HO_2 production and is neutral in the RO_2 budget as explained above. Published rate constants of the second category range between 8×10^{-12} cm^3 s^{-1} and 1.1×10^{-11} cm^3 s^{-1} (Jenkin et al., 2019). Here, the lower limit is almost equal to the rate coefficient of CH_3O_2 (first class). As a sensitivity test, Figs. S5 and S6 show the budgets of ROx, RO_2 and HO_2 for a rate constant of 1×10^{-11} cm^3s^{-1} (R8 + R14). The results are essentially the same as in Figs. 2 and 3 where a rate constant of 9×10^{-12} cm^3 s^{-1} was applied. As the RO_2 budget indicates a missing RO_2 sink, a larger rate constant could help resolve the discrepancy. However, the 10% increase of the rate constant for R8 + R14 in Figs. S5 and S6 is far too small to explain the observed imbalance.

The reaction of RO_2 radicals with NO can form HO_2 (reaction R8) resulting in radical-chain propagation, or produce organic nitrates (reaction R14) resulting in chain termination. As the branching ratio can be different for each RO_2 species and as most of the organic reactivity was caused by unmeasured VOCs, the branching ratios of most RO_2 species are not known. Typical yields for organic nitrates lie in the range between 1% and 35% (Atkinson, 1982; Lightfoot et al., 1992). For the budget analysis (Figs. 2-4), an organic nitrate yield of 5% is assumed. Figs. S7 and S8 show cases where higher yields (10%, 20%) are assumed. Higher organic nitrate yields compensate the slightly negative bias of *D-P* in the RO_x budget (Fig. S7). An average yield of 10% would lead to a perfect balance between production and destruction rate of ROx during daytime, whereas a yield of 20% would result in a slightly positive bias of up to +1 ppbv/h in *D-P*. For the HO_2 production rate, these changes have little impact. Thus, in all cases (80%, 90%, 95% yield of HO_2), the HO_2 budget is balanced within the experimental uncertainties.

Published rate constants for the reaction RO_2+HO_2 (R16) lie in the range between 0.5×10^{-11} cm^3 s^{-1} and 2.2×10^{-11} cm^3 s^{-1} at 298K (Jenkin et al., 2019). In MCM, a general value of 2.3×10^{-11} cm^3 s^{-1} (298K) is assumed and scaled by an RO_2 specific factor which is typically 0.5 - 0.7. In the budget analysis we have used the upper limit with a scaling factor of one. Thus, the possible bias of the calculated RO_2+HO_2 rate is in the order of a factor of 2. Under the polluted conditions of the campaign, the loss of RO_2 and HO_2 is largely dominated by NO. The reaction RO_2+HO_2 contributes only a few percent to the ROx loss during daytime and no more than 10% at sunset, when NO is small. Thus, the bias in the calculated ROx loss rate remains well below 5% at daytime. Similar considerations apply to the loss of RO_2 and HO_2, which is also dominated by NO during the day.

Rate coefficients for self and cross reactions of RO_2 are diverse and difficult to parameterize (Jenkin et al., 2019). The rate constants for the most abundant species are generally an order of magnitude smaller than for the reaction R16 (RO_2+HO_2). Self reactions of oxygenated RO_2 and cross reactions of some RO_2 can be as fast as reaction R16 (Jenkin et al., 2019). Overall, RO_2+RO_2 reactions play a smaller role than RO_2+HO_2 reactions in the Heshan campaign. The uncertainty of the RO_2 radical budget due to the lumped rate coefficient for R15 is therefore negligible.

References:

Atkinson, R., Lloyd, A. C., and Winges, L.: An updated chemical mechanism for hydrocarbon/NOx/SO2 photooxidations suitable for inclusion in atmospheric simulation models, Atmos. Environ., 16, 1341-1355, https://doi.org/10.1016/0004-6981(82)90055-5, 1982.

Jenkin, M. E., Valorso, R., Aumont, B., and Rickard, A. R.: Estimation of rate coefficients and branching ratios for reactions of organic peroxy radicals for use in automated mechanism construction, Atmos. Chem. Phys. Discuss., 2019, 1-46, https://doi.org/10.5194/acp-2019-44, 2019.

Lightfoot, P. D., Cox, R. A., Crowley, J. N., Destriau, M., Hayman, G. D., Jenkin, M. E., Moortgat, G. K., and Zabel, F.: Organic peroxy radicals: Kinetics, spectroscopy and tropospheric chemistry, Atmos. Environ., 26, 1805-1961, https://doi.org/10.1016/0960-1686(92)90423-I, 1992.

Osthoff, H. D., Roberts, J. M., Ravishankara, A. R., Williams, E. J., Lerner, B. M., Sommariva, R., Bates, T. S., Coffman, D., Quinn, P. K., Dibb, J. E., Stark, H., Burkholder, J. B., Talukdar, R. K., Meagher, J., Fehsenfeld, F. C., and Brown, S. S.: High levels of nitryl chloride in the polluted subtropical marine boundary layer, Nature Geoscience, 1, 324-328, 10.1038/ngeo177, 2008.

Tan, Z. F., Fuchs, H., Lu, K. D., Hofzumahaus, A., Bohn, B., Broch, S., Dong, H. B., Gomm, S., Haseler, R., He, L. Y., Holland, F., Li, X., Liu, Y., Lu, S. H., Rohrer, F., Shao, M., Wang, B. L., Wang, M., Wu, Y. S., Zeng, L. M., Zhang, Y. S., Wahner, A., and Zhang, Y. H.: Radical chemistry at a rural site (Wangdu) in the North China Plain: observation and model calculations of OH, HO2 and RO2 radicals, Atmos. Chem. Phys., 17, 663-690, https://doi.org/10.5194/acp-17-663-2017, 2017.

Tham, Y. J., Wang, Z., Li, Q., Yun, H., Wang, W., Wang, X., Xue, L., Lu, K., Ma, N., Bohn, B., Li, X., Kecorius, S., Größ, J., Shao, M., Wiedensohler, A., Zhang, Y., and Wang, T.: Significant concentrations of nitryl chloride sustained in the morning: investigations of the causes and impacts on ozone production in a polluted region of northern China, Atmos. Chem. Phys., 16, 14959-14977, https://doi.org/10.5194/acp-16-14959-2016, 2016.

Wang, H., Lu, K., Guo, S., Wu, Z., Shang, D., Tan, Z., Wang, Y., Le Breton, M., Lou, S., Tang, M., Wu, Y., Zhu, W., Zheng, J., Zeng, L., Hallquist, M., Hu, M., and Zhang, Y.: Efficient N2O5 uptake and NO3 oxidation in the outflow of urban Beijing, Atmos. Chem. Phys., 18, 9705-9721, 10.5194/acp-18-9705-2018, 2018.

Wang, T., Tham, Y. J., Xue, L., Li, Q., Zha, Q., Wang, Z., Poon, S. C. N., Dubé, W. P., Blake, D. R., Louie, P. K. K., Luk, C. W. Y., Tsui, W., and Brown, S. S.: Observations of nitryl chloride and modeling its source and effect on ozone in the planetary boundary layer of southern China, J. Geophys. Res., 121, 2476-2489, https://doi.org/10.1002/2015JD024556, 2016.

Table S1 Measured quantities used to evaluate the radical budgets.

Measured quantity	Measurement technique	Time resolution	Detection limit [a]	Accuracy (1σ)
OH	LIF [b]	300 s	3.9×10^{5}cm^{-3}	±13 %
HO_2	LIF [b, c]	300 s	1.2×10^{7}cm^{-3}	±20 %
RO_2	LIF [b, c]	300 s	0.6×10^{7}cm^{-3}	±26 %
$RO_2^{\#}$ [d]	LIF [b, c]	300 s	1.7×10^{7}cm^{-3}	±32 %
k_{OH}	LP-LIF [e]	180 s	0.3 s^{-1}	±10 %, ±0.7 s^{-1}
Photolysis frequencies	Actinic flux spectroradiometry	20 s	f	±10 %
O_3	UV photometry	60 s	0.5 ppbv	±5 %
NO	Chemiluminescence	60 s	60 pptv	±20 %
NO_2	Chemiluminescence [g]	60 s	300 pptv	±20 %
HONO	LOPAP [h]	30 s	7 pptv	±20 %
CO,CH_4,CO_2,H_2O	Cavity ringdown spectroscopy	60 s	i	j
SO_2	Pulsed UV fluorescence	60 s	0.1 ppbv	±5 %
HCHO	Hantzsch fluorimetry	60 s	25 pptv	±5 %
NMHCs [k]	GC-FID/MS [l]	1 h	20 - 300 pptv	±(15-20) %

[a] Signal to noise ratio = 1; [b] Laser-induced fluorescence; [c] Chemical conversion via NO reaction before detection; [d] $RO_2^{\#}$ are organic peroxy radicals from large alkanes (> C4), alkenes (including isoprene) and aromatics; [e] Laser photolysis – laser-induced fluorescence; [f] Five orders of magnitude lower than maximum at noon; [g] Photolytic conversion to NO before detection, home built converter; [h] Long-path absorption photometry; [i] CO: 1 ppbv; CH_4:1 ppbv; CO_2: 25 ppbv; H_2O: 0.1 % (absolute water vapor content).; [j] CO: ±1 ppbv; CH_4: ±1 ppbv; CO_2: ±25 ppbv; H_2O: ±5 % ; [k] NMCHs include C_2-C_{11} alkanes, C_2-C_6 alkenes, C_6-C_{10} aromatics; [l] Gas chromatography equipped with mass spectrometer and a flame ionization detector.

Table S2 Measured volatile organic compounds.

Groups	VOC compounds
Alkanes	CYCLOHEXANE, CYCLOPENTANE, ETHANE, I-BUTANE, I-PENTANE, METHYLCYCLOHEXANE, METHYLCYCLOPENTANE, N-BUTANE, N-DECANE, N-DODECANE, N-HEPTANE, N-HEXANE, N-NONANE, N-OCTANE, N-PENTANE, N-UNDECANE, PROPANE, 2,2,4-TRIMETHYLPENTANE, 2,2-DIMETHYLBUTANE, 2,3,4-TRIMETHYLPENTANE, 2,3-DIMETHYLBUTANE, 2,3-DIMETHYLPENTANE, 2,4-DIMETHYLPENTANE, 2-METHYLHEPTANE, 2-METHYLHEXANE, 2-METHYLPENTANE, 3-METHYLHEPTANE, 3-METHYLHEXANE, 3-METHYLPENTANE
Alkenes	CIS-2-PENTENE, CIS-BUTENE, ETHENE, I-BUTENE, PROPENE, TRANS-2-BUTENE, TRANS-2-PENTENE, 1-BUTENE, 1-HEXENE, 1-PENTENE, STYRENE [a]
Aromatics	BENZENE, ETHYLBENZENE, I-PROPYLBENZENE, M-DIETHYLBENZENE, M-ETHYLTOLUENE, M,P-XYLENE, N-PROPYLBENZENE, O-ETHYLTOLUENE, O-XYLENE, P-DIETHYLBENZENE, P-ETHYLTOLUENE, TOLUENE, 1,2,3-TRIMETHYLBENZENE, 1,2,4-TRIMETHYLBENZENE, 1,3,5-TRIMETHYLBENZENE
Alkynes	ETHYNE
Biogenics	ISOPRENE
OVOCs	FORMALDEYHYDE

[a] Styrene is treated as alkene because its major functional group is the C=C double bond with respect to OH reaction.

Supplementary Figures

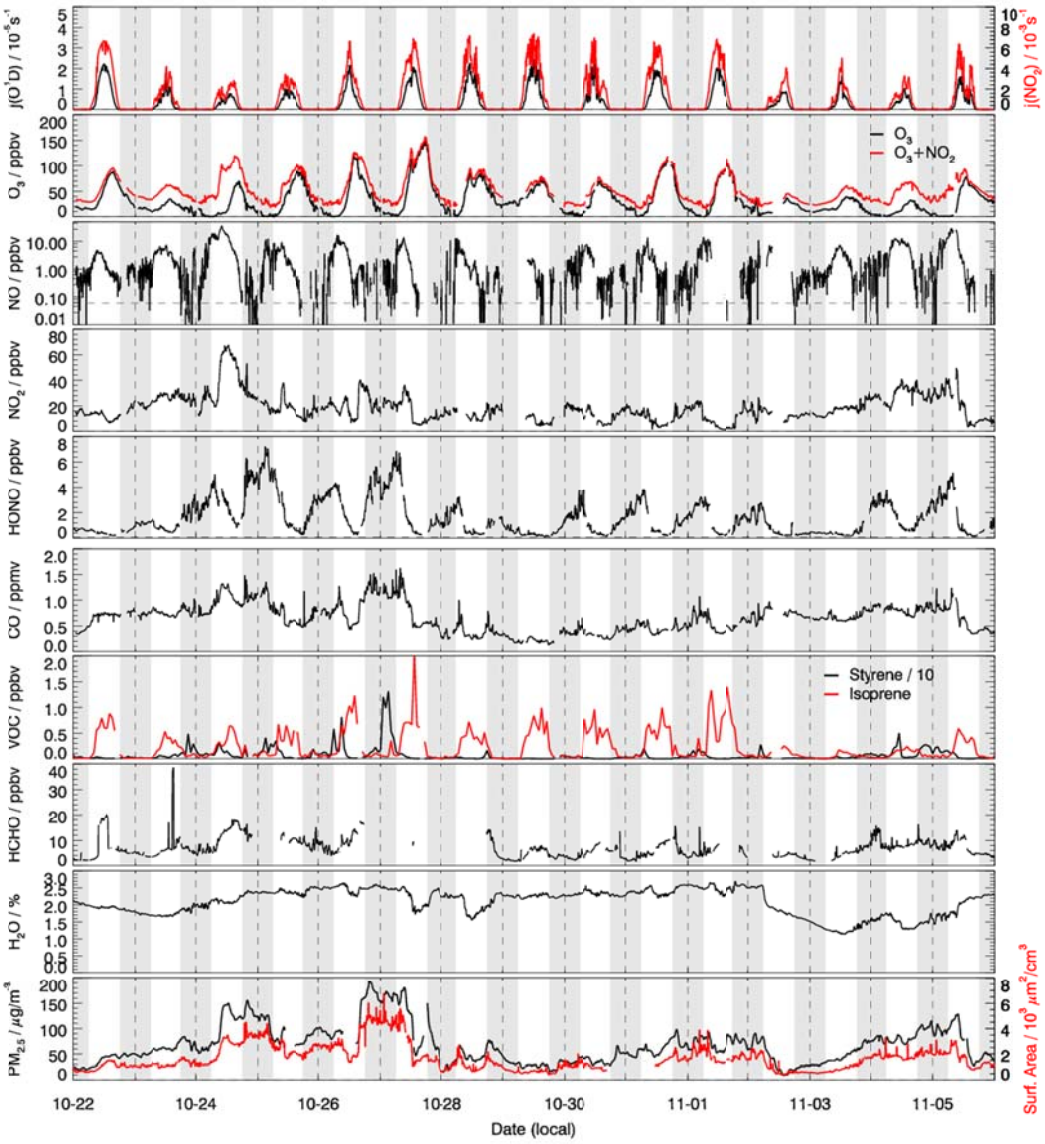

Figure S1. Time series of measured photolysis frequencies, O_3, O_x (O_3+NO_2), NO, NO_2, HONO, CO, isoprene, styrene, HCHO, and H_2O volume mixing ratios, $PM_{2.5}$ mass concentrations and surface area of particulate matter. The vertical dashed lines represent midnight and grey areas represent nighttime.

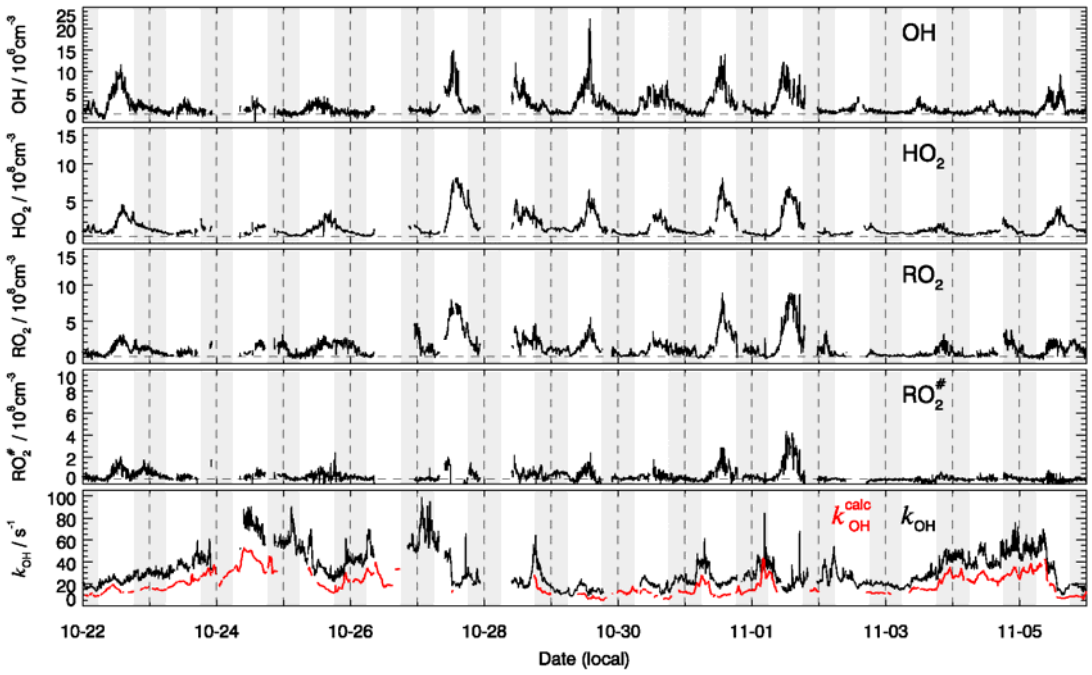

Figure S2. Time series of measured OH, HO_2, RO_2 and $RO_2^{\#}$ concentrations. The lowest panel shows the measured total OH reactivity (k_{OH}) and the calculated OH reactivity (k^{calc}_{OH}) derived from measured concentrations of CO, NO_x, CH_4, NMHCs and HCHO. The vertical dashed lines represent midnight and grey areas represent nighttime.

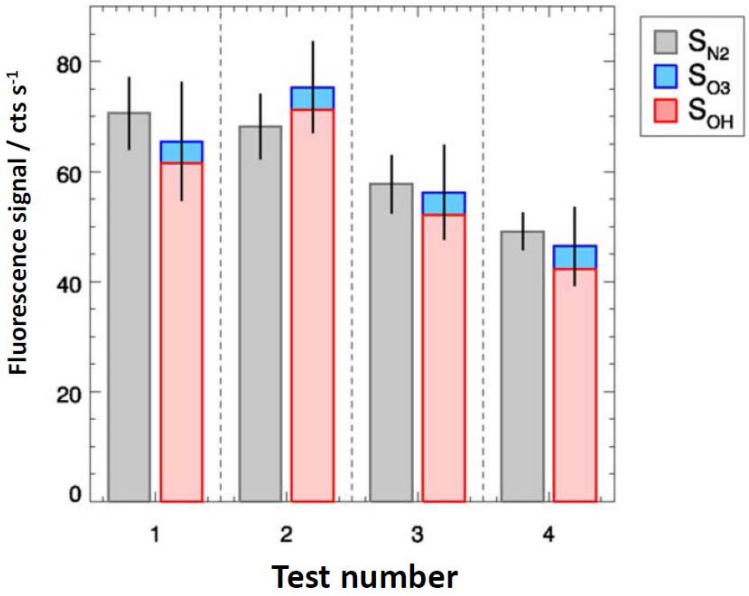

Figure S3. Results from the chemical modulation tests performed on 31 October 2014 between 12:50 and 13:50. The measured OH signal without scavenger (S_{N2}) can be explained within experimental errors by the sum of the signal from ambient OH (S_{OH}) and the known interference from O_3 (S_{O3}). Error bars denote 1σ statistical errors. S_{OH} is calculated by the expression (S_{N2} - $S_{propane}$)/ε, where $S_{propane}$ is the signal with scavenger (propane) and ε is the efficiency of scavenging (for details, see Tan et al., 2017). A fluorescence signal of 60 cts/s is equivalent to an OH concentration of 1×10^{7} cm^{-3}.

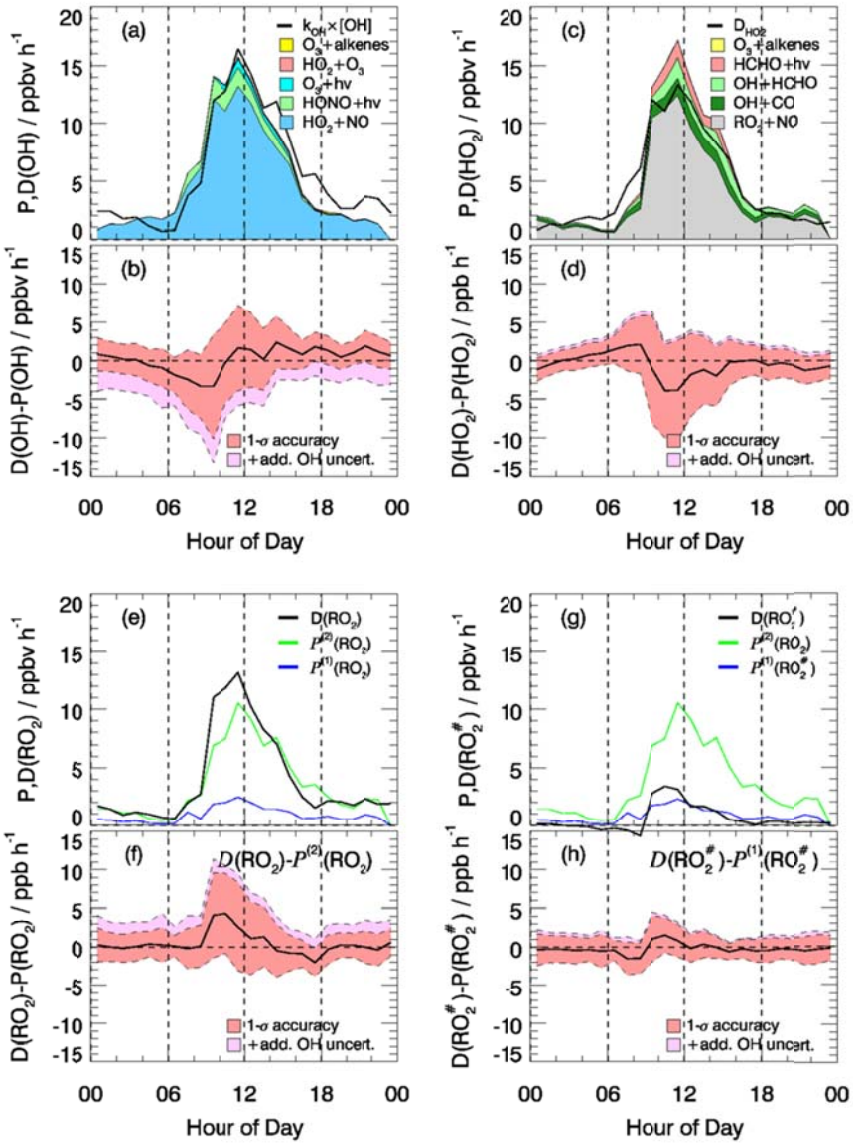

Figure S4. Same as Fig. 3, but with additional RO_2 conversion to OH assuming a first-order rate coefficient of 0.08 s^{-1}. This scenario can also be seen as an application of the X mechanism which recycles OH by the hypothetical sequence $RO_2 + X \rightarrow HO_2$, $HO_2 + X \rightarrow HO_2$ with X equivalent to 0.4 ppbv NO.

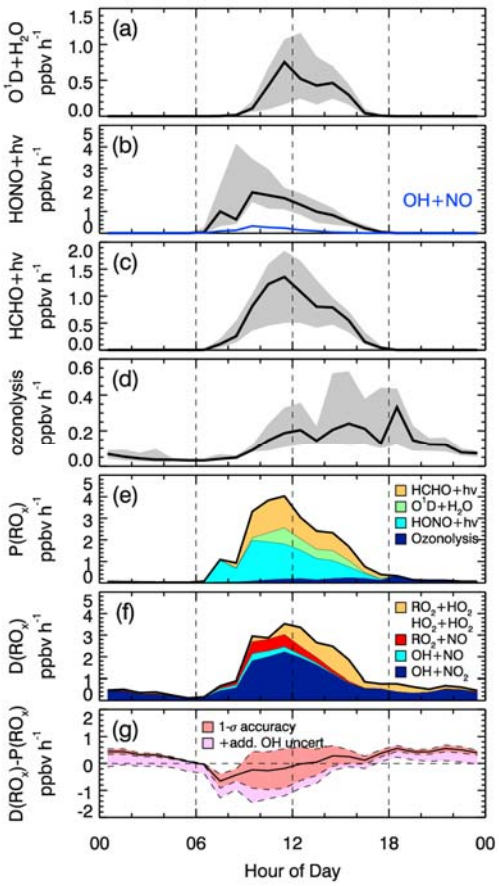

Figure S5. Same as Fig. 2, but assuming a rate constant of 1×10^{-11} cm^{-3} s^{-1} for the reaction of RO_2 with NO (R8 + R14) .

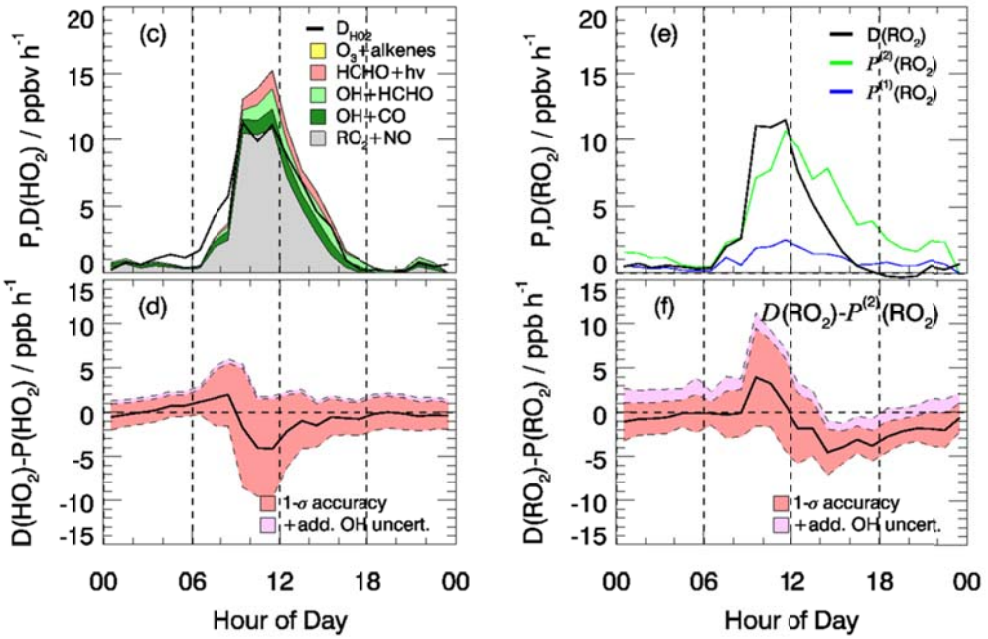

Figure S6. Same as Fig 3c, d, e, f, but assuming a rate constant of 1×10^{-11} cm^{-3} s^{-1} for the reaction of RO_2 with NO (R8 + R14) .

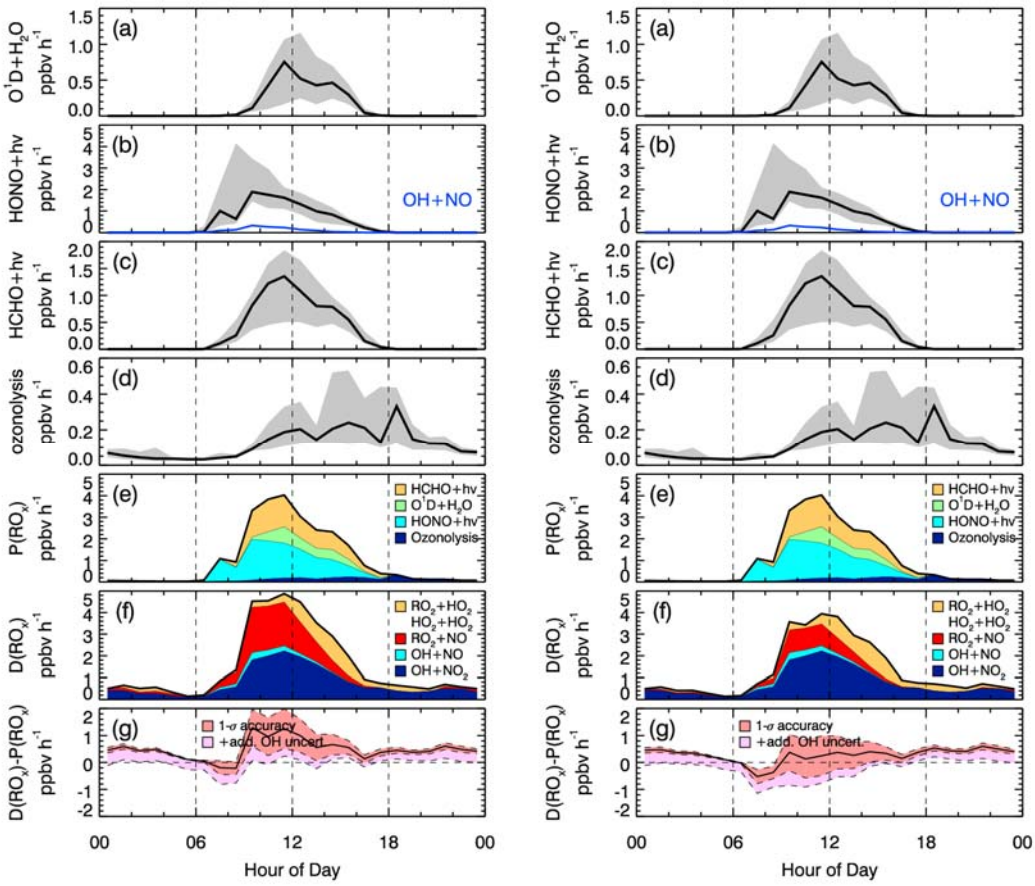

Figure S7. Same as Fig. 2, but assuming a different branching ratio between reaction R8 and R14. Left: HO_2 yield is 0.8, organic nitrate yield is 0.2. Right: HO_2 yield is 0.9, organic nitrate yield is 0.1.

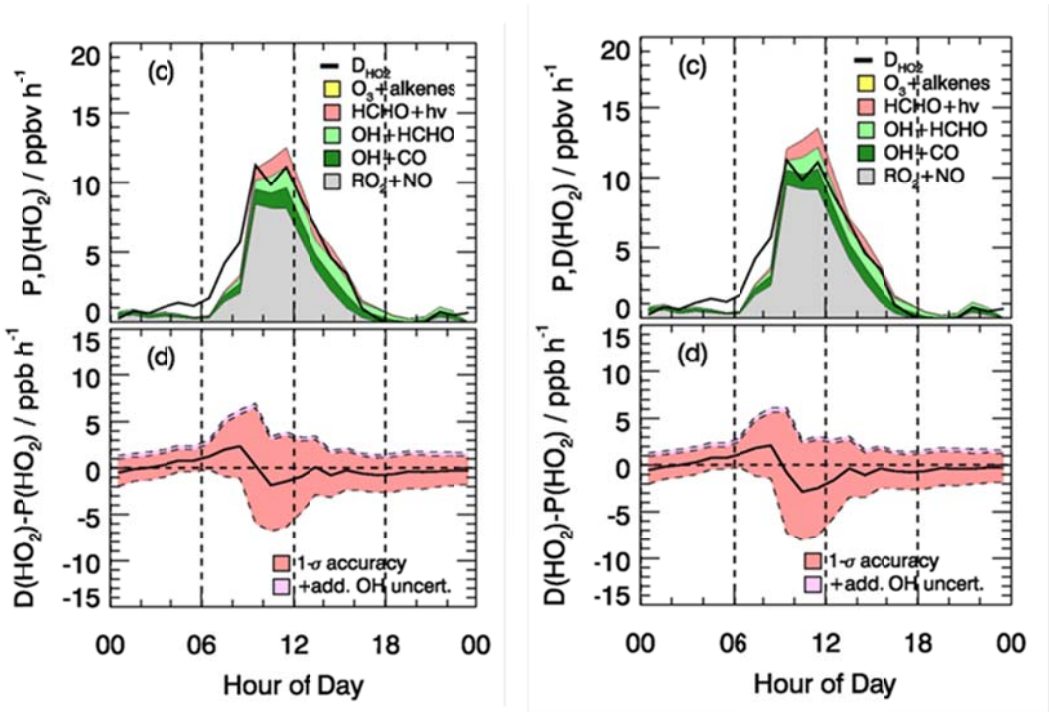

Figure S8. Same as Fig. 3c, d, but assuming a different branching ratio between reaction R8 and R14. Left: HO_2 yield is 0.8, organic nitrate yield is 0.2. Right: HO_2 yield is 0.9, organic nitrate yield is 0.1.